CSPα-deficiency causes massive and rapid photoreceptor degeneration

Frank Schmitz*†‡§, Lucia Tabares‡¶, Darina Khimich‖, Nicola Strenzke‖, Pedro de la Villa-Polo, Manuel Castellano-Muñoz¶, Anna Bulankina‖, Tobias Moser‖, Rafael Fernández-Chacón¶, and Thomas C. Südhof†§**

*Institut für Anatomie und Zellbiologie, Universität des Saarlandes Homburg/Saar, Homburg, 66421 Saarland, Germany; †Center for Basic Neuroscience, Department of Molecular Genetics, and Howard Hughes Medical Institute, University of Texas Southwestern Medical Center, Dallas, TX 75390; ¶Departamento de Fisiología Médica y Biofísica, Universidad de Sevilla, 41009 Sevilla, Spain; ‖Center for Molecular Physiology of the Brain and Department of Otolaryngology, University of Göttingen, 37075 Göttingen, Germany; and **Departamento Fisiología, Universidad de Alcalá, 28871 Madrid, Spain

Contributed by Thomas C. Südhof, December 5, 2005

Cysteine string protein (CSP) α is an abundant synaptic vesicle protein that contains a DNA-J domain characteristic of Hsp40-type cochaperones. Previous studies showed that deletion of CSPα in mice leads to massive lethal neurodegeneration but did not clarify how the neurodegeneration affects specific subpopulations of neurons. Here, we analyzed the effects of the CSPα deficiency on tonically active ribbon synapses of the retina and the inner ear. We show that CSPα-deficient photoreceptor terminals undergo dramatic and rapidly progressive neurodegeneration that starts before eye opening and initially does not affect other retinal synapses. These changes are associated with progressive blindness. In contrast, ribbon synapses of auditory hair cells did not exhibit presynaptic impairments in CSPα-deficient mice. Hair cells, but not photoreceptor cells or central neurons, express CSPβ, thereby accounting for the lack of a hair-cell phenotype in CSPα knockout mice. Our data demonstrate that tonically active ribbon synapses in retina are particularly sensitive to the deletion of CSPα and that expression of at least one CSP isoform is essential to protect such tonically active synapses from neurodegeneration.

hair cell | ribbon synapse | electroretinogram | chaperone | blindness

Synaptic vesicle exo- and endocytosis is mediated by a sophisticated machinery that allows nerve terminals to operate at high speed (1). Such continuous membrane traffic requires specific mechanisms to deal with the use-dependent aging and denaturation of proteins. One such mechanism may involve the synaptic vesicle protein cysteine string protein (CSP) α that is thought to function as a cochaperone in presynaptic terminals (2, 3).

CSPα is an abundant presynaptic protein (4) that contains a string of cysteine residues and a DNA-J domain that functionally collaborates with the DNA-K domains of Hsc70 proteins (reviewed in refs. 5 and 6). CSPα activates the ATPase activity of Hsc70 (7, 8) and forms a trimeric complex with Hsc70 and the tetratricopeptide repeat protein SGT (3). This complex catalyzes the ATP-dependent refolding of denatured luciferase (3). Invertebrates have a single CSP gene, whereas mammals express three CSP genes: CSPα that is widely distributed but highly enriched in brain, and CSPβ and CSPγ that are primarily found in testis (2).

Analyses of knockout (KO) mice revealed that CSPα-deficient mice are relatively normal at birth but exhibit a progressive lethal phenotype that results in death after 2–4 months (2). Recordings in the Calyx of Held synapse of CSPα KO mice documented that CSPα is not required for N-, P/Q-, and R-type Ca^{2+}-channel function or Ca^{2+}-triggered vesicle exocytosis. Instead, in the absence of CSPα, the calyx synapse developed an age-dependent functional impairment, consistent with a role for CSPα as part of a molecular chaperone that makes it possible for synapses to keep running for extended time periods (2). Although this hypothesis was in agreement with previous observations in CSP-deficient flies (4), alternative hypotheses about the function of CSP were proposed based on the phenotype of CSP-deficient flies and on biochemical studies of protein–protein interactions mediated by CSP (7–14).

To further investigate the role of CSPα in synapses, we have now examined the effect of CSPα deficiency on photoreceptor synapses of the retina and on afferent synapses of cochlear inner hair cells. Both synapses are ribbon synapses that are specialized for continuous and high-throughput presynaptic exocytosis (for a review, see refs. 15–17). Our data demonstrate that overall, photoreceptor synapses develop normally in CSPα KO mice but subsequently undergo massive and rapid degeneration that results in total blindness. Ribbon synapses of inner hair cells, however, do not exhibit a similar neurodegeneration, but were found to contain another CSP isoform (CSPβ) that compensates for the loss of CSPα.

Results

Visual Responses in CSPα KO Mice Monitored by Electroretinograms (ERGs). We recorded ERGs in littermate wild-type and CSPα KO mice at postnatal day (P) 14 (immediately after eye opening), P18, P30, and P45 (Fig. 1 *A–C* and data not shown) and determined mean values of the maximum scotopic a- ($a_{max,scot}$) and b-wave amplitudes ($b_{max,scot}$) (Fig. 1*D*).

At P14, a-waves and oscillatory potentials in the ERG were observed in all CSPα-KO mice tested, although the a-wave amplitude was reduced to $\approx$40% of littermate control mice (Table 1, which is published as supporting information on the PNAS web site) and exhibited a slower time course (Fig. 1*A*). The early part of the a-wave mainly reflects the activation of photoreceptor cells (18), whereas oscillatory potentials monitor inner retinal activity (19). Different from the a-wave, the b-wave was absent in four of the five CSPα KO mice tested, and very small in the remaining CSPα KO mouse. Because the b-wave monitors the synaptic activity of photoreceptor synapses in the outer plexiform layer (OPL) (20, 21), these findings suggest that CSPα KO mice primarily have a synaptic photoreceptor defect.

At P18, three of eight CSPα KO mice presented with a flat ERG, whereas the remaining five mice exhibited small and slow a- and b-waves (Fig. 1*B*). The apparent improvement in visual responses at P18 in some CSPα KO mice may be related to the normal increment of the ERG response from P14 to P18 (see wild-type ERG wave amplitudes in Fig. 1*D*), indicating that the progressive degeneration in CSPα KO mice that causes the

Conflict of interest statement: No conflicts declared.

Abbreviations: CSP, cysteine-string protein; ERG, electroretinogram; KO, knockout; OPL, outer plexiform layer; P*n*, postnatal day *n*.

‡F.S. and L.T. contributed equally to this work.

§To whom correspondence may be addressed. E-mail: frank.schmitz@uniklinik-saarland.de or thomas.sudhof@utsouthwestern.edu.

 www.pnas.org/cgi/doi/10.1073/pnas.0510060103

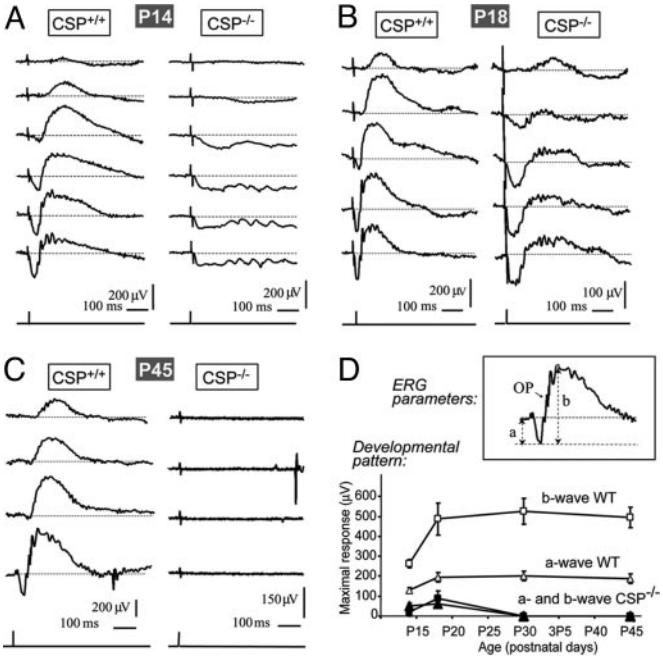

Fig. 1. ERG analysis of retinal function in wild-type and CSPα KO mice. Dark-adapted eyes of wild-type (CSP$^{+/+}$) and CSPα KO (CSP$^{-/-}$) mice were stimulated with single flashes of light of increasing energy, and mixed rod/cone responses were recorded by ERG. (*A–C*) Representative responses recorded at P14 (*A*), P18 (*B*), and P45 (*C*) are displayed. Each trace represents the average response to light intensities from −0.1 to 2.44 log cd·sec/m^2 recorded in 8 trials. (*D*) The maximal scotopic a- and b-wave amplitudes in wild-type and CSPα KO mice at P14, P18, P30, and P45 are depicted to illustrate where the respective waves were measured.

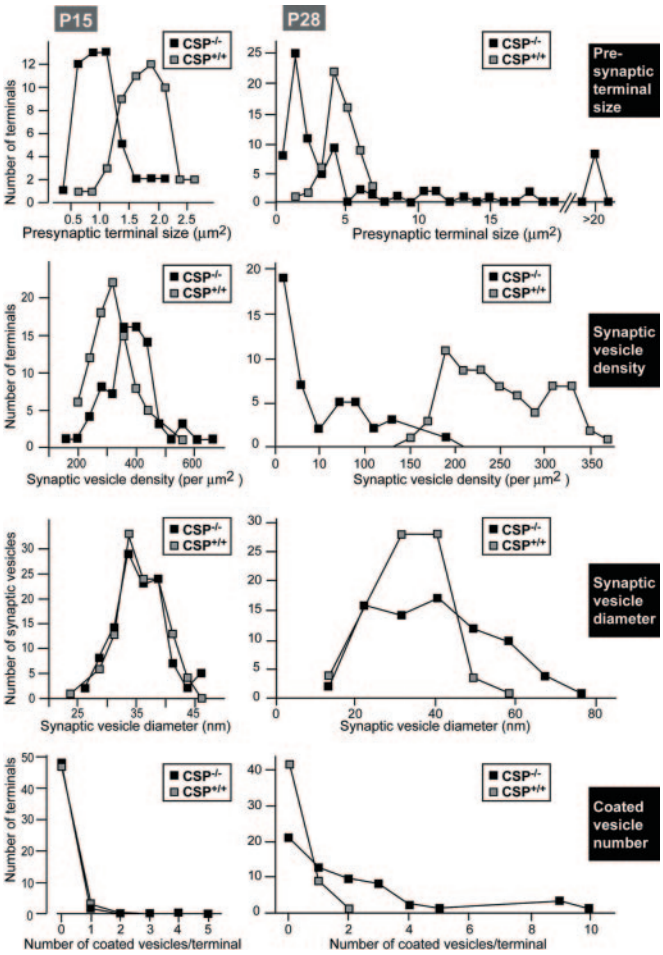

Fig. 2. Quantitation of key parameters of photoreceptor nerve terminals from littermate wild-type and CSPα KO mice at P15 (*Left*) and P28 (*Right*). At P15, synaptic vesicle diameter and coated vesicle number were indistinguishable between wild-type and CSPα KO synapses. In CSPα KO mice, we observed an increase in the synaptic vesicle density in comparison to wild-type mice and a decrease in the presynaptic terminal size. Dramatic quantitative changes were observed at P28 between wild-type and CSPα KO mice. We observed strong scattering in the size of the presynaptic terminals in CSPα KO mice with part of the terminals being smaller than the average wild-type photoreceptor ribbon synapse and with part of the presynaptic terminals being extremely big. The CSPα KO mice displayed a strong decrease in synaptic vesicle density, a broader distribution in the size of synaptic vesicle size, and an increase in the number of coated vesicles.

functional impairment proceeds in parallel with the physiological reorganization and maturation of the retina. In CSPα KO mice with a measurable ERG response at P18, the time to peak of the a-wave was almost three times longer (38–78 ms) than in wild-type littermate control mice (10–20 ms), revealing an abnormally slow light response (Fig. 1*B*). The onset of oscillatory potentials was also slower in CSPα KO than in wild-type mice (Fig. 1 *A* and *B*). At P30 and P45, all CSPα KO mice lacked a detectable ERG response (Fig. 1 and Table 1). These data suggest that CSPα KO mice initially have some visual function but suffer from progressive blindness that completely abolishes vision after 4 weeks of age. The difference in visual responses at P18 probably reflects a variability in the onset of retinal dysfunction between mice. The functional impairment of photoreceptors in CSPα-deficient mice was present both in rod and cone synapses (Fig. 6, which is published as supporting information on the PNAS web site).

Structure of Photoreceptor Synapses in Young CSPα KO Mice. In the period before eye opening, at P4-P5, the OPL, which contains the photoreceptor ribbon synapses, is in the process of being formed and synaptic proteins start to accumulate (22). No obvious light microscopic changes in the distribution of synaptic proteins, and no major changes in the ultrastructural appearance of photoreceptor ribbon synapses were observed at this age between wild-type and CSPα KO mice (Fig. 7, which is published as supporting information on the PNAS web site). Also after eye opening, at P15, when the OPL has been formed (22), no dramatic differences between CSPα KO and wild-type mice were observed in the distribution of synaptic proteins as well as in the ultrastructural appearance of ribbon synapses (Fig. 8, which is published as supporting information on the PNAS web site). However, quantitation of synaptic features at P15 revealed that the presynaptic photoreceptor ribbon terminals were smaller in mutant than in wild-type littermate control mice and exhibited an increased synaptic vesicle density (Fig. 2).

Degenerating Photoreceptor Ribbon Synapses in Adult CSPα KO Mice. In contrast to the discrete morphological changes at P15, we observed dramatic morphological changes at P28 in the OPL of CSPα KO mice. Immunofluorescence microscopy revealed that synaptic vesicle proteins at P28 were no longer restricted to the OPL in CSPα KO mice (Fig. 3). The continuous array of synaptic ribbons of the OPL was disrupted, and ectopic ribbons and synaptic proteins were detected also in the outer nuclear layer. The abundance of synaptic membrane proteins in the OPL was decreased for nearly all synaptic proteins analyzed. At P28, also nonsynaptic proteins (e.g., opsin) were mislocalized (Fig. 9, which is published as supporting information on the PNAS web site). These changes appeared to be largely restricted to the OPL

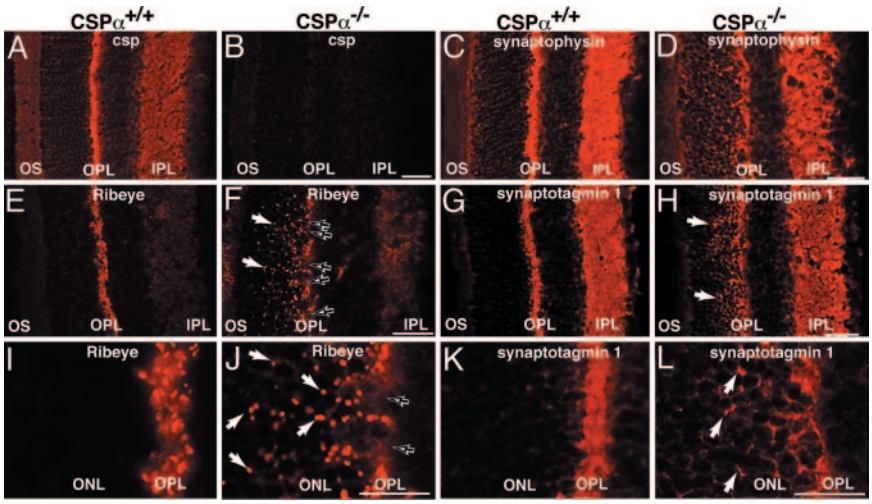

Fig. 3. Distribution of synaptic proteins in the retina from wild-type and CSPα KO mice at P28. Cryostat sections of CSP-wild-type (*A*, *C*, *E*, *G*, *I*, and *K*) and CSPα KO mice (*B*, *D*, *F*, *H*, *J*, and *L*) stained with antibodies to CSP (*A* and *B*), synaptophysin (*C* and *D*), RIBEYE (*E*, *F*, *I*, and *J*), and synaptotagmin 1 (*G*, *H*, *K*, and *L*). *I–L* are higher magnification views to illustrate that synaptic proteins were no longer restricted to their physiological localization in the OPL of CSPα KO mice: In mutant mice, synaptic ribbons and synaptic proteins were partly found at abnormal localization in the ONL (arrows in *F*, *H*, *J*, and *L*). In *F*, black arrows point to a discontinuously labeled OPL. OS, outer segments, ONL, outer nuclear layer; IPL, inner plexiform layer. (Scale bars: *A–H*, 30 μm; *I–L*, 15 μm.)

where photoreceptor ribbon synapses are located, whereas the distribution of synaptic proteins in the inner plexiform layer in the inner retina was not detectably altered. At P28, we additionally observed aberrant sprouting of secondary retinal neurons and activation of Müller glial cells (Fig. 10, which is published as supporting information on the PNAS web site), common features in retinal neurodegeneration as consequence of photoreceptor death (e.g., refs. 23 and 24).

At the ultrastructural level, most of the ribbon synapses in the OPL of CSPα KO mice displayed a strongly pathological morphology, although occasionally normal appearing ribbon synapses were detected (<5%; Figs. 4 *D–H* and Fig. 11, which is published as supporting information on the PNAS web site). Higher magnification electron micrographs revealed heterogeneous and pleomorphic alterations of photoreceptor ribbon synapses that ranged from a strong decrease in synaptic vesicle density (Fig. 4 *D–H*), a change in synaptic architecture (strong decrease or loss of the invaginated shape of the presynaptic plasma membrane; Fig. 4 *D*, *G*, and *H*), formation of electron-dense aggregates (Fig. 4*E*) and detachment of the synaptic ribbon ("floating" synaptic ribbons, Fig. 4 *G* and *H*) to a complete loss of synaptic ribbons from presynaptic photoreceptor terminals (Fig. 4*D*). In strongly degenerated cases, large electron-lucent presynaptic terminals contained few synaptic vesicles, but many coated vesicles (Fig. *4 F–H* and 9), and featured floating synaptic ribbons. Strongly degenerated terminals were often found close to less severely affected terminals. Quantitation revealed that all synaptic parameters analyzed were severely altered (Fig. 2). As observed at P15, most of the terminals at P28 were smaller in CSPα KO mice than in littermate controls, but terminal sizes were much more heterogeneous, and large swollen terminals accounted for a significant percentage of the total. The density of synaptic ribbon-containing presynaptic terminals was strongly reduced [wild-type mice: 0.50 $\pm$ 0.16 ribbon-containing ribbon synapses/μm OPL (n = 20); CSPα KO mice: 0.11 $\pm$ 0.08 ribbon-containing ribbon synapses/μm OPL (n = 20)], and the membrane-attachment of ribbons was decreased [wild-type animals: 90% docked ribbons (n = 75); CSPα KO mice: 38% docked ribbons (n = 75)]. Probably secondary to the synaptic changes, we also found structural alterations of photoreceptor outer segments in CSPα-deficient mice at P28 (Fig. 11). No obvious phenotype was observed in bipolar cell ribbon synapses or in conventional chemical synapses of the inner retina (data not shown).

Normal Morphology and Function of Ribbon Synapses in Inner Hair Cells of CSP KO Mice. Immunostaining of afferent inner hair cell synapses for presynaptic ribbons and postsynaptic glutamate receptors revealed comparable numbers of ribbon-containing afferent synapses in wild-type and CSPα-deficient inner hair cells [Fig. 5 *A* and *B*; wild-type mice: 10.8 $\pm$ 1.3 ribbon-containing synapses per hair cell (n = 21); CSPα KO mice: 12.6 $\pm$ 0.5 synapses per cell (n = 26)]. Next we performed patch-clamp measurements of Ca^{2+} currents and exocytic capacitance changes in inner hair cells by using step depolarizations to -5 mV for 5, 20, and 50 ms to probe L-type Ca^{2+} currents and the fast and sustained phases of inner hair cell exocytosis (25, 26). We did not detect significant differences in the exocytic capacitance changes or Ca^{2+} current amplitudes between wild-type and CSPα mice (Fig. 5*C*; see also Fig. 12, which is published as supporting information on the PNAS web site; wild-type: n = 17; KO: n = 13).

We next tested hearing in CSPα KO mice (*Supporting Methods*, which is published as supporting information on the PNAS web site). At 4 weeks of age, we found in CSPα KO mice a mild hearing impairment of $\approx$30 dB, accompanied by a reduction or loss of otoacoustic emissions (Fig. 12). To focus on potential effects of the CSPα deficiency that originate from hair cell ribbon synapses and not from central auditory processing, we analyzed mice with only comparable otoacoustic emissions, but detected no significant difference in the first peak of auditory brainstem responses (which reflects spiral ganglion activation by transmitter release at the hair cell ribbon synapses) between matched CSPα KO and wild-type mice (Figs. 5 and 12).

The lack of a major defect in ribbon synapses of inner hair cells in CSPα KO mice was puzzling until we observed that CSP immunoreactivity persisted in these cells in CSPα KO mice, even though it was absent in efferent axodendritic synapses underneath the inner hair cells (Fig. 5 *E* and *F*). Therefore we analyzed mouse inner hair cells for expression of additional CSP isoforms that might compensate for the loss of CSPα. RT-PCR with mRNA from the entire organ of Corti showed expression of CSPα and CSPβ (Fig. 5*G*), whereas only CSPα was expressed in the retina (Fig. 5*G*, n = 3 experiments for each organ). Single-

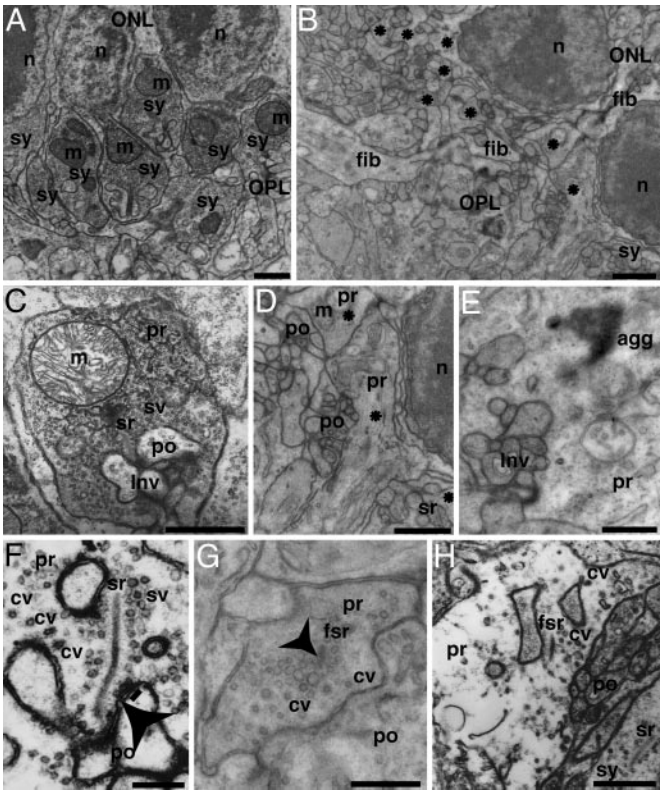

Fig. 4. Electron micrographs of ribbon synapses in the OPL from wild-type (*A* and *C*) and CSPα KO mice (*B* and *D–H*) at P28. Low magnification views (*A* and *B*) show dense and regular arrangement of ribbon synapses (sy) in the OPL close to the ONL in wild-type mice (*A*) but not in CSPα KO mice (*B*) in which degenerated ribbon synaptic complexes are found in the OPL (asterisks). The neuropil in the OPL of mutant mice was increased, with processes (fib) crossing the OPL and sprouting into the ONL (*B*). High-magnification views (*C–H*) in wild-type retina (*C*) show a typical ribbon synapse with an invaginated presynaptic terminal. In contrast, photoreceptor ribbon synapses from CSPα KO mice displayed a pathological morphology (*D–H*) with decreased synaptic vesicle density (*D–H*) and with electron-dense aggregates in some terminals (*E*). The arrowhead in *F* points to an omega-shaped exocytosis figure in a moderately degenerated ribbon terminal with three docked synaptic vesicles nearby (underlined). In the most severely degenerated presynaptic terminals (*F* and *H*; see also Fig. 9), presynaptic terminals are large and electron-lucent with few synaptic vesicles but many coated vesicles (cf. *F* and *H*). ONL, outer nuclear layer; sy, ribbon synapse; n, nucleus; m, mitochondria; Inv, invagination of the postsynaptic dendrites into the presynaptic terminal; cv, coated vesicles; fsr floating (detached) synaptic ribbon; agg, electron dense aggregate; fib, sprouting process; pr, presynaptic; po, postsynaptic. (Scale bars: *A–D*, 1 μm; *E–H*, 500 nm.)

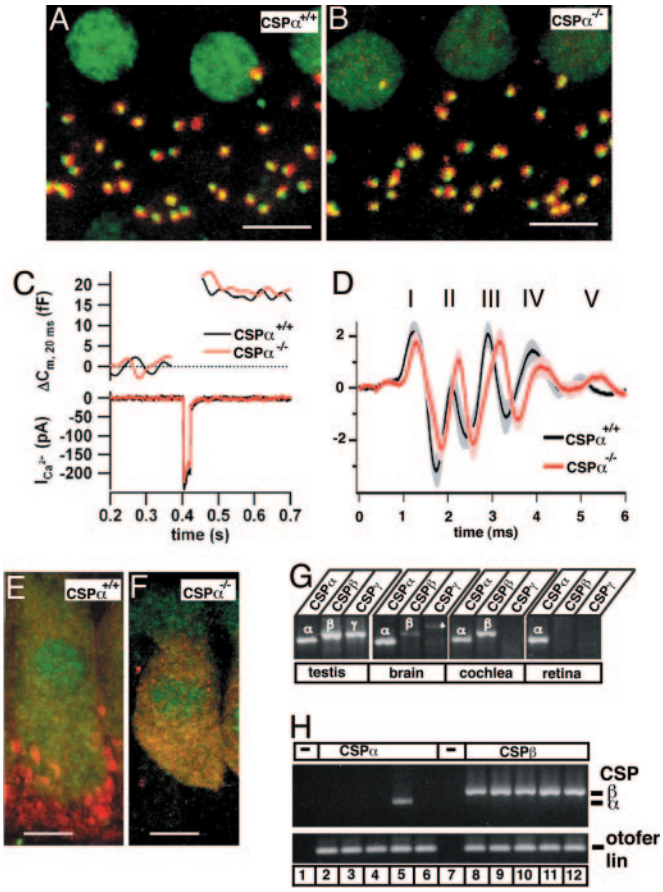

Fig. 5. CSPα-deficient hair cell ribbon synapses are morphologically and functionally unchanged. (*A* and *B*) Representative immunofluorescence images of inner hair cells from wild-type (*A*) and CSPα KO (*B*) mice stained with antibodies to RIBEYE (green) and glutamate receptors (red). Pictures show Z projections of confocal stacks through four neighboring inner hair cells (Scale bar: 5 μm.). (*C*) representative Ca^{2+} current ($I_{Ca^{2+}}$) and capacitance traces (C_m) from wild-type and CSPα KO inner hair cells stimulated by a 20-ms step depolarization. (*D*) Average auditory brainstem responses ($\pm$SEM) evoked by suprathreshold clicks (80 dB per sound pressure level) in 4- to 6-week old wild-type ($n = 9$) and CSPα KO ($n = 12$) mice. Numbers denominate the wild-type auditory brainstem response peaks. (*E* and *F*) Inner hair cells of wild-type (*E*) and CSPα KO (*F*) immunostaining for CSP (red, isoform unspecific polyclonal antibody) and calbindin (green). Note the red boutons at the base of the hair cell in the wild-type image, which represent efferent presynaptic terminals (as identified by costaining for synaptophysin, data not shown) that contain CSPα only. (*G*) RT-PCR products obtained with isoform-specific primers for CSPα, CSPβ, and CSPγ from cDNA of testis, brain, cochlea, and retina. Testis expressed all CSP isoforms, brain, and cochlea were positive for CSPα and CSPβ, whereas retina only expressed CSPα. The asterisk in the CSPγ PCR in the brain denotes an additional, unrelated band that may represent a primer amplification artifact. (*H*) Single-cell RT-PCR of inner hair cells performed with primers specific for CSPα (lanes 2–6; 1 of 5 positive) and CSPβ (lanes 8–12; all positive). Amplification of cDNA of the inner hair-cell specific protein otoferlin was used as a positive control. No PCR products were observed in the negative controls (lane 1 and 7).

cell RT-PCR (Fig. 5*H*) confirmed the expression of CSPβ in inner hair cells (21 of 21 cells), whereas CSPα was detected only infrequently (7 of 24 cells). Therefore CSPβ instead of CSPα appears to be the major CSP isoform in inner hair cells. In contrast, in the retina, CSPα was the only expressed CSP isoform as judged both at the mRNA level (by using RT-PCR) and the protein level (Fig. 13, which is published as supporting information on the PNAS web site).

Discussion

Our results reveal that deletion of CSPα causes early onset, rapidly progressive degeneration of photoreceptors in the mouse retina. Both rod and cone photoreceptor responses, as monitored by ERGs, became abnormal immediately after eye opening (at P14; Figs. 1 and 6). Initially, the ERG b-wave was more severely depressed than the a-wave, suggesting that the dysfunction starts in presynaptic photoreceptor terminals (Fig. 1). Two weeks later, the mice were blind, and no ERG responses could be elicited.

Parallel to the ERG changes, we noted structural changes in photoreceptor ribbon synapses immediately after eye opening. At P15, the size of the photoreceptor terminals selectively decreased $\approx$2-fold without a loss of synaptic vesicles or other changes (Figs. 2 and 8; see also Fig. 14, which is published as supporting information on the PNAS web site). These initial abnormalities rapidly progressed to fulminant neurodegenera-

tion in CSPα KO mice at ≈P28 when almost all photoreceptors were degenerated (Figs. 3, 4, 9, and 11). Retinal photoreceptor degeneration was selective in that no other retinal synapse, including ribbon synapses formed by bipolar neurons, exhibited major signs of neurodegeneration at P28 in CSPα KO mice; however, other frequently used synapses elsewhere (e.g., the neuromuscular junction and the calyx synapse) were also degenerating at this time in development (2).

Although at P28 photoreceptors were largely degenerated and visual function abolished in CSPα KO mice, hair cell ribbon synapses appeared unaffected (Fig. 5). Auditory brainstem responses revealed a mild hearing impairment and delayed conduction of auditory information, consistent with the previously observed synaptic degeneration in the auditory brainstem (2). The hearing impairment of CSPα-deficient mice coincided with a reduction or loss of otoacoustic emissions and was probably caused in part by a defect in middle ear sound transduction (*Supporting Methods*). The continued function of hair cell ribbon synapses in CSPα KO mice was initially surprising until we noticed that different from photoreceptors and central synapses (where CSPα appears to be the only CSP isoform present; ref. 2), inner hair cells express CSPβ. It thus seems likely that CSPβ in inner hair cells compensates for the lack of CSPα and protects the hair cells from neurodegenerative changes. The differential expression of CSP isoforms adds to already described differences in the molecular makeup of auditory and visual ribbon synapses (e.g., refs. 27 and 28).

The retinal degeneration in CSPα KO mice gives clues to the function of CSP.

The selectivity of the neurodegeneration (i.e., the preferential degeneration of photoreceptors) shows that different types of neurons exhibit differential sensitivity to the loss of CSPα. In central and retinal neurons, this difference cannot be attributed to the coexpression of other CSP isoforms because RT-PCR experiments and immunoblotting/immunocytochemistry analyses (with antibodies that recognize all CSP-isoforms; ref. 2) failed to detect other CSP isoforms (Figs. 3, 5, and 13). Because photoreceptor synapses are tonically active, their preferential sensitivity to the CSPα deletion is probably caused by the continuous use of the synaptic release machinery. This explanation agrees well with the early degeneration of neuromuscular junctions and calyx synapses that are also strongly used synapses (2). Ribbon synapses of bipolar neurons were much less affected than photoreceptor ribbon synapses, possibly because the impairment in photoreceptors decreased their overall synaptic input, thereby making bipolar ribbon synapses less dependent on CSPα-chaperone activity.

Neurodegeneration of photoreceptors in CSPα KO mice appears to proceed in an almost stochastic manner. During the neurodegeneration, apparently healthy terminals are adjacent to completely degenerated terminals. Even at P28, some terminals still look normal. A similar phenomenon was previously observed at the calyx synapse (2). This finding suggests that a neuron can compensate for the loss of CSPα for a limited time with an apparently normal appearance.

Finally, quantitation of the ultrastructural features indicated that photoreceptor terminals shrink at P15, before the photoreceptors overtly degenerate (Fig. 2), at the same time at which the ERG exhibited a primary impairment in the b-wave that is due to photoreceptor synaptic transmission (Fig. 1). At later stages, pervasive morphological abnormalities were detected, consistent with the notion that the degeneration starts in the photoreceptor terminals, and initially impairs membrane traffic in the terminals with later changes in the overall terminal structure.

Viewed together, our data support the hypothesis that CSPα is not required for synaptic function as such, not even in synaptic photoreceptor terminals because some visual responses are retained at P14, but is essential for keeping nerve terminals alive in an activity-dependent manner. Such a use-dependent function is consistent with a role for CSPα as a cochaperone that ensures the native folding of unknown substrates. Although the identity of these substrates is unknown, one major and early change in CSPα-deficient neurons, before degeneration sets in, is a loss of the SNARE protein SNAP-25, indicating that SNARE proteins may be involved in the degeneration (29). Thus, SNARE proteins are prime candidates as direct or indirect CSPα substrates because they are abundant presynaptic proteins that are continuously assembled and disassembled into complexes during presynaptic function and could potentially be toxic in a nonfolded form.

Materials and Methods

Miscellaneous. All analyses were performed with at least three independently derived littermate CSPα KO and wild-type mice obtained from heterozygous matings between P5 and P50. Mice were genotyped by PCR as described in ref. 2 or alternatively by using the primers MCM1 (ACT GTT AAA GAG ACT GTC ATG AAA AAGG) and MCM2 (GGG GGA GGG AAT GTG GGT GAG TGT AGT TAG) for the wild-type reaction.

ERGs. ERGs were recorded with a bio-amplifier (A.D. Instruments), sampled at 2–10 kHz, filtered with a bandpass of 0.1 Hz-1000 Hz, and averaged and analyzed with POWERLAB software (A.D. Instruments); for details of the ERG recordings, see *Supporting Methods*. All numerical data were analyzed by the two-tailed Student *t* test.

Patch-Clamp Recordings. Inner hair cells were patch-clamped in the perforated-patch configuration; membrane capacitance (C_m) measurements were made as described in ref. 25 (see also *Supporting Methods*). C_m changes were calculated as the difference of post- and prestimulus C_m, averaged for a given cell, and presented as an overall average over several cells.

Indirect Immunofluorescence Microscopy. (*i*) Retina: Immunofluorescence labeling was performed as described in ref. 30 by using previously characterized antibodies (22, 27, 31–33); note that the CSPα antibody used (2) crossreacts with all CSP isoforms. (*ii*) Hair cells: Organs of Corti were fixed with 4% paraformaldehyde in 120 mM Na-phosphate buffer (1 h). After incubation of whole-mount preparations (1 h) in 16% normal goat serum/450 mM NaCl/0.3% Triton X-100/20 mM phosphate buffer, pH 7.4, primary antibodies were applied overnight at 4°C. The following antibodies were used: mouse anti-CtBP2/RIBEYE B-domain (BD Biosciences, 1:100–200), rabbit anti-GluR2/3 (Chemicon, 1:1,000), and rabbit anti-calbindin (Swants, 1:100). Secondary Alexa Fluor-labeled antibodies (Molecular Probes, 1:200) were applied for 1 h. Confocal images were collected and quantified as described in ref. 26.

Electron Microscopy. Electron microscopy and quantitations of electron micrographs was performed as described in ref. 34. Ultrathin sections were analyzed with a Zeiss EM902 or with a digital Biotwin 12 Tecnai electron microscope (FEI) equipped with morphometric software (SIS).

We thank J. Craatz, C. Franke, I. Benito, M. Degenhardt, M. Koeppler, and C. de Cires for excellent technical assistance; M. L. Montesinos and I. Roux for primer sequences; and Dr. G. Alvarez de Toledo for support and advice. The study was supported by Deutsche Forschungsgemeinschaft Grants Schm797/5-5 and SFB530, TP C11 (to F.S.); FEDER Grants BFI2001-4959-E (European Molecular Biology Organization Young Investigator Programme), BFI2002-01686 (to R.F.-C.), BFI2004-00350, and BFI2001-3199 (to L.T.); the Institute of Health Carlos III BEFI Fellowship 01/9310 (to M.C.-M.); and grants by the Center for Molecular Physiology of the Brain (to T.M.), Human Frontiers Science Program and European Commission (Eurohear) (to T.M.), the Spanish Ministry of Science and Technology (to R.F.-C.), and the Göttingen University (to N.S.).

1. Südhof, T. C. (2004) *Annu. Rev. Neurosci.* **27,** 509–547.
2. Fernández-Chacón, R. F., Wölfel, M., Nishimune, H., Tabares, L., Schmitz, F., Castellano-Muñoz, M., Rosenmund, C., Montesinos, M. L., Sanes, J. R., Schneggenburger, R. & Südhof, T. C. (2004) *Neuron* **42,** 237–251.
3. Tobaben, S., Thakur, P., Fernandez-Chacon, R., Südhof, T. C., Rettig, R. & Stahl, B. (2001) *Neuron* **31,** 987–999.
4. Zinsmaier, K. E., Hofbauer, A., Heimbeck, G., Pflugfelder, G. O., Buchner, S. & Buchner, E. (1990) *J. Neurogenet.* **7,** 15–29.
5. Kelley, W. L. (1998) *Trends Biochem. Sci.* **23,** 222–227.
6. Hartl, F. U. & Hayer-Hartl, M. (2002) *Science* **295,** 1852–1858.
7. Braun, J. E., Wilbanks, S. M. & Scheller, R. H. (1996) *J. Biol. Chem.* **271,** 25989–25993.
8. Chamberlain, L. H. & Burgoyne, R. D. (1997) *Biochem. J.* **322,** 853–858.
9. Gundersen, C. B. & Umbach, J. A. (1992) *Neuron* **9,** 527–537.
10. Brown, H., Larrson, O., Branstrom, R., Yang, S. N., Leibiger, B., Leibiger, I., Fried, G., Moede, T., Deeney, J. T., Brown, G. R., *et al.* (1998) *EMBO J.* **17,** 5048–5058.
11. Leveque, C., Pupier, S., Marqueze, B., Geslin, L., Kataoka, M., Takahashi, M., De Waard, M. & Seagar, M. (1998) *J. Biol. Chem.* **273,** 13488–13492.
12. Dawson-Scully, K., Bronk, P., Atwood, H. L. & Zinsmaier, K. E. (2000) *J. Neurosci.* **20,** 6039–6047.
13. Graham, M. E. & Burgoyne, R. D. (2000) *J. Neurosci.* **20,** 1281–1289.
14. Magga, J. M., Jarvis, S. E., Arnot, M. I., Zamponi, G. W. & Braun, J. E. (2000) *Neuron* **28,** 195–204.
15. Von Gersdorff, H. (2001) *Neuron* **29,** 7–10.
16. Fuchs, P. A., Glowatzki, E. & Moser, T. (2003) *Curr. Opin. Neurobiol.* **13,** 452–458.
17. Sterling, P. & Matthews, G. (2005) *Trends Neurosci.* **28,** 20–29.
18. Penn, R. D. & Hagins, W. A. (1969) *Nature* **223,** 201–204.
19. Wachtmeister, L. (1998) *Prog. Retin Eye Res.* **17,** 485–521.
20. Robson, J. G. & Frishman, R. J. (1998) *Doc. Ophthalmol.* **95,** 187–215.
21. Shiells, R. A. & Falk, G. (1999) *Vis. Neurosci.* **16,** 503–511.
22. Von Kriegstein, K. & Schmitz, F. (2003) *Cell Tissue Res.* **311,** 159–173.
23. Jones, B. W., Watt, C. B., Frederick, J. M., Baehr, W., Chen, C. K., Levine, E. M., Milam, A. H., Lavail, M. M. & Marc, R. E. (2003) *J. Comp. Neurol.* **461,** 1–16.
24. Dick, O., tomDieck, S., Altrock, W. D., Ammermüller, J., Weiler, R., Garner, C. C., Gundelfinger, E. D. & Brandstätter, J. H. (2003) *Neuron* **37,** 775–786.
25. Moser, T. & Beutner, D. (2000) *Proc. Natl. Acad. Sci. USA* **97,** 883–888.
26. Khimich, D., Nouvian, R., Pujol, R., tomDieck, S., Egner, A., Gundelfinger, E. D. & Moser, T. (2005) *Nature* **434,** 889–894.
27. Von Kriegstein, K., Schmitz, F., Link, E. & Südhof, T. C. (1999) *Eur. J. Neurosci.* **11,** 1335–1348.
28. Safieddine, S. & Wenthold, R. J. (1999) *Eur. J. Neurosci.* **11,** 803–812.
29. Chandra, S., Gallardo, G., Fernandez-Chacon, R., Schlüter, O. M. & Südhof, T. C. (2005) *Cell* **123,** 383–396.
30. Schmitz, F., Bechmann, M. & Drenckhahn, D. (1996) *J. Neurosci.* **16,** 7109–7116.
31. Schmitz, F., Königstorfer, A. & Südhof, T. C. (2000) *Neuron* **28,** 857–872.
32. Shaw, G. & Weber, K. (1983) *Eur. J. Cell Biol.* **30,** 219–232.
33. Lewis, G. P. & Fisher, S. K. (2003) *Int. Rev. Cytol.* **230,** 263–290.
34. Schoch, S., Castillo, P. E., Jo, T., Mukherjee, K., Geppert, M., Wang, Y., Schmitz, F., Malenka, R. C. & Südhof, T. C. (2002) *Nature* **415,** 321–326.